Equivalent Circuit Approximation to Porous Mixed-Conducting Oxygen Electrodes in Solid-State Cells

Meilin Liu*

School of Materials Science and Engineering, Georgia Institute of Technology, Atlanta, Georgia 30332-0245, USA

ABSTRACT

While porous mixed ionic-electronic conductors (MIECs) have been widely used as electrodes for solid-state ionic devices, the electrochemical processes occurring in such an electrode are still not well understood. Equivalent circuit analyses indicate that there are three parallel paths for electrode reactions to occur in a cell with porous MIEC electrodes: (*i*) the triple-phase boundary (TPB) between the electrolyte, the MIEC, and O_2 gas, (*ii*) the TPB between the current collector, the MIEC, and O_2 gas, and (*iii*) the interface between the MIEC and O_2 gas. The relative significance of each path is determined not only by the transport and catalytic properties of the MIEC but also by the interfaces between the MIEC and other cell components. The effectiveness of the MIEC/gas interface is influenced by the rates of several sequential processes: transfer of ionic defects across the MIEC/electrolyte interface, transport of ionic and electronic defects in the MIEC, reaction at the MIEC/gas interface, and transport of O_2 in the pores of the MIEC. Accordingly, oxygen diffusion in the MIEC and reaction at the MIEC/gas interface are only part, not the entirety, of the electrode kinetics. In general, the TPBs cannot be ignored without careful analysis or adequate justification. Further, as a first-order approximation, it is demonstrated that the thickness of the electrochemically active layer of a porous MIEC electrode, δ, varies dramatically with the properties of the MIEC. Typically, δ decreases with increased rate of surface reaction and with decreased transport of ionic or electronic defects in the MIEC. In the absence of ionic or electronic transport in the MIEC, for instance, δ approaches zero, i.e, oxygen reduction or evolution can occur only at one of the TPBs.

Introduction

It is well recognized[1] that, in contrast to an electrode of a pure electronic conductor (such as Pt), an electrode formed from a mixed ionic-electronic conductor (MIEC) has the potential to extend the reaction sites or zones beyond the triple-phase boundaries (TPBs) between the electrode, electrolyte, and O_2 gas. Accordingly, MIECs have been widely used as electrodes for solid-state ionic devices (e.g., solid oxide fuel cells, batteries, and gas sensors) and for electrochemical processes (e.g., gas separation or electrosynthesis).[2-6] However, the detailed reaction paths and electrode kinetics in cells with porous MIEC electrodes are still not well understood. A recent model,[7] for instance, predicts that the impedance of a cell with porous MIEC electrodes (of infinite thickness and uniform Fermi level) is determined merely by the properties of the MIEC, oxygen diffusivity in the MIEC and surface catalytic properties, and is independent of the properties of the interfaces between the MIEC and other cell components (electrolyte and current collector). This prediction, first of all, directly contradicts experimental observations; recent impedance spectroscopy studies[8] demonstrate that the impedances of cells based on different electrolyte materials but with same MIEC electrodes are influenced dramatically by the interfaces between the MIEC and the electrolyte. Second, our analyses[9] indicate that, in addition to the reactions at MIEC/gas interface, other reaction paths through the TPBs are an important part of the electrode kinetics and cannot be ignored without careful analysis and adequate justification.

In this paper, equivalent circuit analysis demonstrates conclusively that, in general, there are three parallel paths for electrode reactions to occur in a cell with porous MIEC electrodes: two types of triple-phase boundaries (TPBs) in parallel to the MIEC/gas interface. It is incorrect to assert that "consideration of a separate parallel three-phase boundary (TPB) reaction would be redundant"[7]; on the contrary, consideration of the TPBs as parallel paths to the MIEC/gas interface is a minimum requirement for any meaningful analysis of a solid-state system. TPBs are inherent to solid-state electrochemical systems and failing to address TPBs will lead to erroneous boundary conditions[9] and ultimately to invalid conclusions.[9] Further, it is demonstrated unequivocally that, for a cell based on MIEC electrodes of infinite thickness and uniform Fermi level, it is the TPB between the electrolyte, the MIEC, and O_2, rather than the bulk phase of the MIEC,[7] that dominates the electrode kinetics and cell impedance, when the impedance of the TPB is smaller than the impedance of any of the following processes: ion transfer across the MIEC/electrolyete interface, oxygen transport in the MIEC, or the reaction at the MIEC/gas interface.

The observations that electrodes of MIECs with high rate of oxygen transport and surface reaction appear to show fast electrode kinetics do not necessarily mean that the oxygen transport in MIEC and surface reaction are the only processes dominating the electrode kinetics. The observed fast electrode kinetics may, for instance, result from enhanced catalytic activity of the TPBs. It should be recognized that the simultaneous transport of ionic and electronic defects in an MIEC electrode may not only extend the reaction sites from TPBs to the MIEC/gas interface, but also enhance the catalytic property of the TPBs. The latter advantage has not be well recognized, particularly when the TPBs are ignored all together.[7]

Clarification of reaction paths in a cell with porous MIEC electrodes is critical to gaining a profound understanding of the electrode kinetics (including the details of the reaction mechanisms) of such an electrode, to correct interpretation of impedance data of cells with such electrodes, and to meaningful modeling and effective design or improvement of porous MIEC electrodes for various applications.

Model Description

Schematically shown in Fig. 1 is a symmetrical cell consisting of a solid electrolyte of a pure ionic conductor (el, $t_i = 1$), two porous electrodes of an MIEC ($0 < t_e < 1$), and two current collectors of a pure electronic conductor (cc, $t_e = 1$). Unless stated otherwise, it is further assumed that (*i*) the electrolyte is essentially homogeneous and there is no significant space charge polarization at grain boundaries,[a] (*ii*) the MIEC electrode contains a continuous porous phase, through which O_2 gas may transport to or away from the TPBs and the MIEC/gas interface, (*iii*) the solid phase of the electrode is a single-phase, homogeneous MIEC (such as $LaFeO_3$- or $LaCoO_3$-based perovskite material) in which local charge neutrality is approximately observed and there is no significant bulk polarization, (*iv*) the electronic conductivity of the current collector is sufficiently greater than the conductivities of other cell

* Electrochemical Society Active Member.

[a] Alternatively, either the grain boundary resistance and capacitance are sufficiently small or the time constant for grain boundary relaxations is much shorter than those for other electrochemical processes occurring in the cell so that their impedance response can be readily separated from the impedance of other processes.

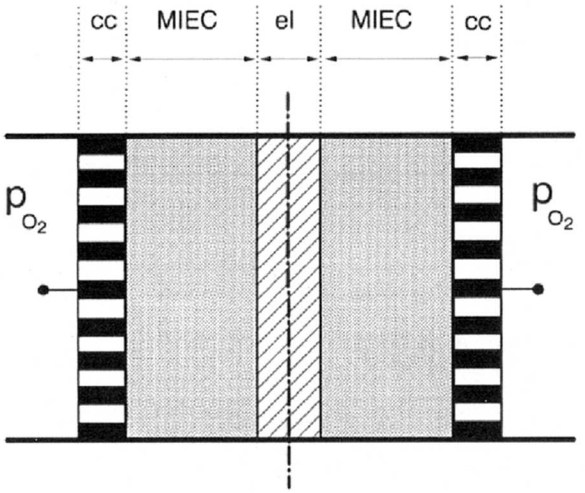

Fig. 1. A schematic diagram showing a symmetrical cell consisting of a solid electrolyte (el), two porous MIEC electrodes, and two current collectors (cc).

components so that the variations in Fermi level in the current collector are negligible, (*v*) the properties of each cell component in a plane perpendicular to the direction x are the statistical average properties on the plane so that the system may be treated as a one-dimensional problem, and (*vi*) all current or mass fluxes are on a superficial area basis. The equations and conclusions derived under these assumptions, however, may be further extended to cells based on a mixed-conducting electrolyte (el, $0< t_e < 1$),[10] as discussed in Appendix A, and to cells based on electrodes of composite MIECs consisting of two or more phases,[11] as discussed in Appendix B. The effect of bulk polarization in the MIEC is also briefly discussed in Appendix B.

Electrochemical processes.—The electrochemical processes which may occur in such a cell are schematically illustrated in Fig. 2 (only half of the cell is shown) and briefly described as follows.

In the electrolyte of uniform composition, the motion of the ionic defects is considered to be pure migration (driven by $\nabla\phi$), i.e.

$$J_i = -\sigma_{i,el}\nabla\phi, \qquad \sigma_{i,el} = \sum_i z_i^2 F^2 u_i c_i \qquad [1a]$$

At the MIEC/el interface ($x = L$), two types of processes can be differentiated: (*i*) the electrochemical reaction occurring at the triple-phase boundary (TPB1) between the el, the MIEC, and the O_2 gas

$$V_O^{\bullet\bullet}(\text{el}) + 2e'(\text{MIEC}) + \frac{1}{2}O_2(\text{gas}) = O_O^{\times}(\text{el}) \qquad [1b]$$

and (*ii*) the transfer of ionic defects (such as $V_O^{\bullet\bullet}$) across the MIEC/el interface

$$V_O^{\bullet\bullet}(\text{el}) = V_O^{\bullet\bullet}(\text{MIEC}) \qquad [1c]$$

In the region of the porous electrode ($0 < x < L$) with porosity p, solid-phase tortuosity τ_s, and gas-phase tortuosity τ_g, three types of processes can be identified: (*i*) the transport of ionic and electronic defects in the solid phase MIEC through diffusion (driven by $\nabla\mu_k$) and migration (driven by $\nabla\phi$)

$$J_k = -z_k F\left(\frac{u_k}{\tau_s}\right)[(1-p)c_k](\nabla\mu_k + z_k F\nabla\phi) = J_{k,\text{diff}} + J_{k,\text{migr}}$$

$$J_T = \sum_k J_k = J_{\text{ion}} + J_{\text{ele}} \qquad [1d]$$

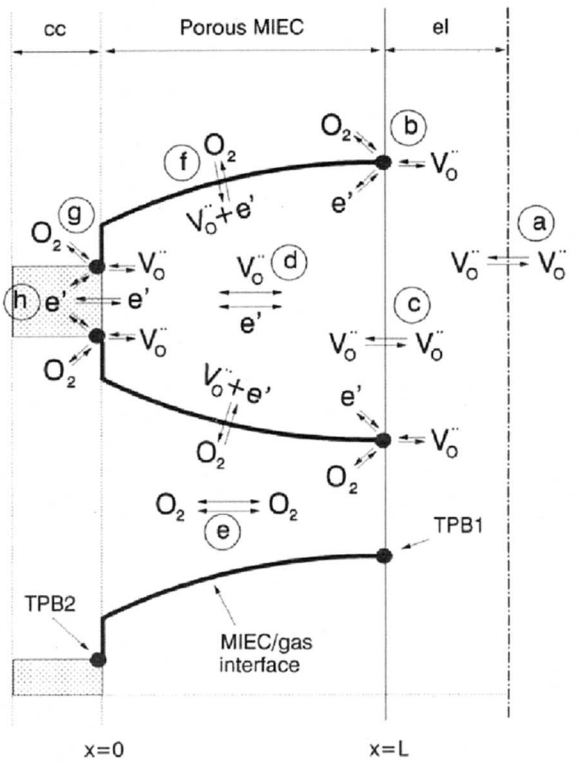

Fig. 2. A schematic diagram showing the electrochemical processes which may occur in the cell shown in Fig. 1 (only half of the cell is shown). The schematic processes labeled with a circled letter, a to h, correspond to the processes described by Eq. 1a to 1h.

(*ii*) the transport of O_2 gas in the pores of the MIEC through diffusion (driven by $\nabla\mu_{O_2}$) and convection (due to the motion of the gas in the pores with a bulk velocity υ)

$$N_{O_2} = \left[-\left(\frac{u_{O_2}}{\tau_g}\right)\nabla\mu_{O_2} + \upsilon\right](pc_{O_2}) \qquad [1e]$$

and (*iii*) the interaction between the O_2 gas and the MIEC at the MIEC/gas interface

$$\{V_O^{\bullet\bullet} + 2e'\}(\text{MIEC}) + \frac{1}{2}O_2(\text{gas}) = O_O^{\times}(\text{MIEC}) \qquad [1f]$$

At the cc/MIEC interface ($x = 0$), three other types of processes can be identified: (*i*) the reaction occurring at the second triple-phase boundary (TPB2) between the cc, the MIEC, and O_2 gas

$$V_O^{\bullet\bullet}(\text{MIEC}) + 2e'(\text{cc}) + \frac{1}{2}O_2(\text{gas}) = O_O^{\times}(\text{MIEC}) \qquad [1g]$$

(*ii*) the transfer of electrons across the cc/MIEC interface

$$e'(\text{MIEC}) = e'(\text{cc}) \qquad [1h]$$

and (*iii*) the reaction at the MIEC/gas interface at $x = 0$, which is the same reaction as described by Eq. 1f.

Current and mass fluxes.—The ionic current flow pattern in the vicinity of the porous MIEC electrode is schematically sketched in Fig. 3a. Part of the ionic flux moving from the electrolyte toward the MIEC/el interface is directly converted to electronic flux by the reaction at the TPB1 (Eq. 1b). The remaining ionic flux, transferred into the MIEC through the MIEC/el interface, is then consumed either by the reaction at the MIEC/gas interface (Eq.1f) or by the reaction at the TPB2 (Eq. 1g), depending primarily on the relative ionic and electronic transport properties of the MIEC, but also influenced by the nature

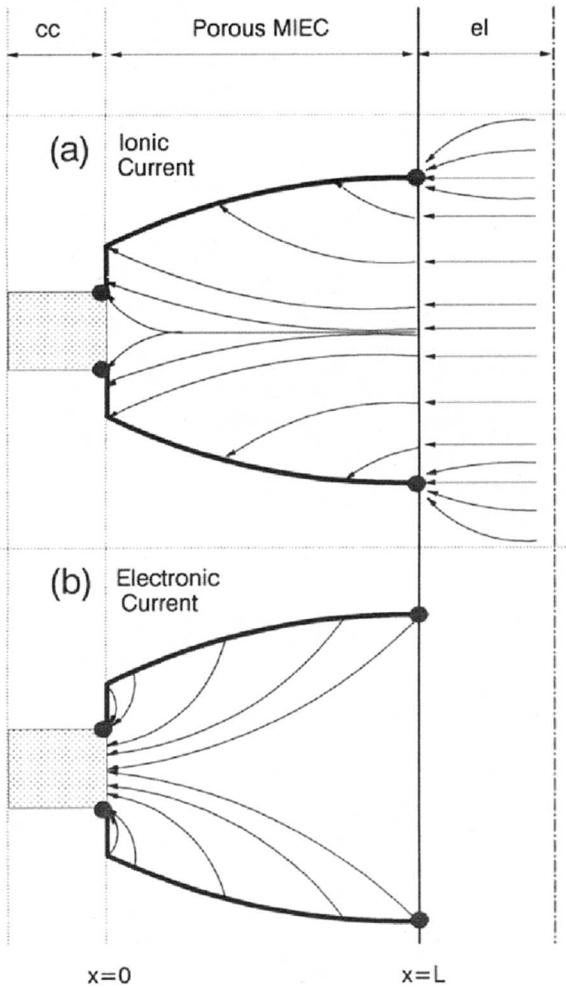

Fig. 3. A schematic diagram showing the flow patterns of (a) ionic and (b) electronic currents in the vicinity of a porous MIEC electrode. Note that the electron holes move in the direction of the electronic current while the electrons move in the direction opposite to the direction of the electronic current.

of the interfaces. Typically, the significance of the reaction at TPB2 increases with increased ionic transport, decreased electronic transport, and with decreased rate of surface reaction. Because of the reaction at TPB1, the steady-state fluxes at the MIEC/el interface ($x = L$) must be balanced as follows

$$[J_{ion}]_{MIEC,x\to L} + J_{TPB1} = [J_{ion}]_{el,x\to L} \quad [2a]$$

$$[J_{ele}]_{MIEC,x\to L} = J_{TPB1} \quad [2b]$$

Schematically sketched in Fig. 3b is the electronic current flow pattern in the solid phase of the porous MIEC electrode. At $x = L$, electronic current is produced at the TPB1 due to the reaction described by Eq. 1b. Then, additional electronic fluxes are generated by the reaction at MIEC/gas interface (Eq. 1f). Finally, any remaining ionic flux at $x = 0$ must be transferred to electronic flux either by the reaction at the TPB2 (Eq.1g) or by the reaction occurring at the MIEC/gas interface (Eq. 1f) at $x = 0$. Accordingly, the steady-state fluxes at the cc/MIEC interface ($x = 0$) must be balanced as follows

$$J_{TPB2} + [2Fr]_{MIEC,x\to 0} = [J_{ion}]_{MIEC,x\to 0} \quad [2c]$$

$$J_T = [J_{ele}]_{MIEC,x\to 0} + J_{TPB2} + [2Fr]_{MIEC,x\to 0} \quad [2d]$$

where r represents the net consumption rate of $V_O^{\bullet\bullet}$ at the MIEC/gas interface and J_T is the total current density as defined by Eq. 1d.

Further, as the ionic current is converted to electronic current or vice versa by the electrode reactions (Eq. 1b, 1f, and 1g), O_2 gas is simultaneously consumed (or generated) at TPB1, MIEC/gas interface, and TPB2; this can be expressed, in a steady state, as

$$J_{ele}(x) = -4FN_{O_2}(x), \quad 0 \le x \le L \quad [2e]$$

Continuous operation of such an electrode, then, requires that the O_2 gas transport to (or away from) these reaction sites through the pores of the MIEC. The rate of O_2 transport in the pores of MIEC may influence the partial pressure of O_2 near or at these reaction sites and hence may influence the rate of the interfacial processes and the impedance response of the interfaces.

Since the MIEC electrode must be porous to allow sufficient gas transport, the ionic current may heavily concentrate on the TPB1 at $x = L$; in fact, all current must pass through the TPB1 when the mobility or concentration of the ionic defects in the electrode vanishes (e.g., when a Pt electrode is used). With the increase in transport of the ionic and electronic defects in the MIEC, the active sites or zones for reduction or evolution of oxygen (Eq. 1b and 1g) may be extended beyond the TPBs to the MIEC/gas interface (Eq. 1f). The degree of extension is primarily determined by the properties of the MIEC and the interfaces. In principle, when the rate of ionic and electronic transport in the MIEC is sufficiently fast in comparison to the rate of the surface reaction, the active reaction sites will be extended to the entire MIEC/gas interface.

The current or flux balances described by Eq. 2a to 2e are true in general for cells with MIEC electrodes; failing to consider TPBs will lead to erroneous boundary conditions, invalid conclusions, and incorrect interpretation of impedance data.[9]

Equivalent circuit.—When the cell is exposed to a uniform atmosphere having oxygen partial pressure of p_{O_2}

$$p_{O_2}, \text{ cc/MIEC/el/MIEC/cc, } p_{O_2}$$

and under the influence of a small ac perturbation, such as in an impedance measurement, the electrochemical behavior of such a cell may be adequately approximated by the equivalent circuit shown in Fig. 4 (only half of the circuit is shown). The porous MIEC electrode is approximated by an electrical transmission line model, which has been widely used to model rough electrode surfaces,[12-14] corroding interfaces,[15] and porous electrodes of an electronic conductor involving liquid electrolytes.[16,17] The transmission line model, however, is properly modified to reflect the fundamental differences between a porous MIEC electrode exposed to a gas and the systems exposed to a liquid studied previously.[b] In the transmission line model shown in Fig. 4a, dR_e, dR_i, and dZ_r represent the impedance, respectively, to electronic transport, ionic transport, and to the reaction at the MIEC/gas interface of an MIEC layer with thickness of dx, at a distance x away from the cc/MIEC interface. Thus, integration along each path for electrochemical processes over the entire bulk phase of the porous MIEC results in three lumped circuit elements, $R_{i,MIEC}$, $R_{e,MIEC}$, and Z_{rt} . The circuit shown in Fig. 4a is then transformed to the one shown in Fig. 4b. The impedance of each circuit element in Fig. 4 is normalized by the superficial area of the porous electrode (thus having dimension of Ω cm^2) and is defined as follows.

In the electrolyte, the resistance to the motion of the ionic defects, $R_{i,el}$, is defined as

$$R_{i,el} = L_{el}/\sigma_{i,el} \quad [3a]$$

[b] First, in a porous MIEC electrode, both ionic and electronic species are transported through the same solid MIEC while in the other electrode, ionic species transport through the liquid electrolytes and electrons move through the solid electronic conductor. Second, the triple-phase boundaries between the electrolyte, the MIEC, and the gas phase are a very important part of the electrode kinetics in a solid-state cell.

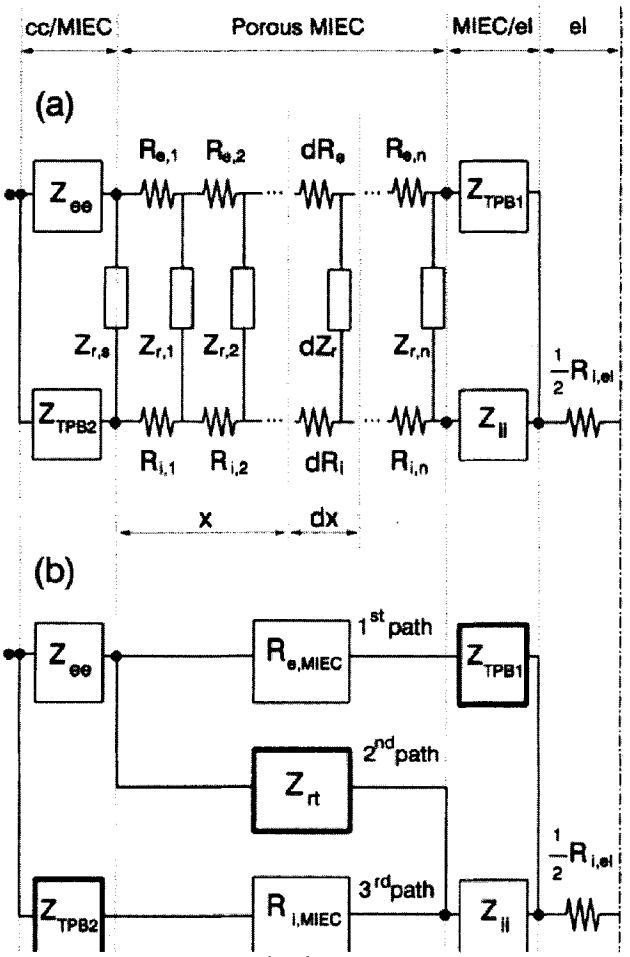

Fig. 4. Equivalent circuits for the cell shown in Fig. 1 under the influence of a small ac perturbation (only half of the circuit is shown): (a) a transmission line model and (b) a simplified model with lumped circuit elements. In the discretized form of the transmission line model (a), $R_{e,m}$ and $R_{i,m}$ ($1 \le m \le n$) represent the resistance to the motion of electronic and ionic defects, respectively, in an arbitrary element m, $Z_{r,m}$ corresponds to the impedance to the charge and mass transfer at or near the MIEC/gas interface of element m, and $Z_{r,s}$ is the impedance to charge and mass transfer at the MIEC/gas interface at $x = 0$. In the simplified circuit (b), the three circuit elements with bold frames (Z_{TPB1}, Z_{rt}, and Z_{TPB2}) represent the impedances to oxygen reduction or evolution at three different types of reaction sites.

where $\sigma_{i,el}$ and L_{el} are the ionic conductivity and the thickness of the electrolyte, respectively. Since the polarization at grain boundaries of polycrystalline electrolyte is assumed to be negligible in order to focus on electrode processes, the impedance response of the electrolyte is approximated by a pure resistance, $R_{i,el}$.

At the MIEC/el interface at $x = L$, the impedance at an angular frequency ω to the electrochemical reactions occurring at the TPB1, $Z_{TPB1}(\omega)$, can be defined as

$$Z_{TPB1}(\omega) = \frac{\partial \eta_{TPB1}(\omega)}{\partial J_{TPB1}(\omega)} = f(p_{O_2}, c_e, c_v, \phi, J_{o,TPB1}, C_{TPB1}) \quad [3b]$$

where η_{TPB1}, J_{TPB1}, $J_{o,TPB1}$, and C_{TPB1} are the overpotential across, the current density passing through, the exchange current density at, and the capacitance of the TPB1, respectively. The relationship between η_{TPB1} and J_{TPB1} can be approximated by the Butler-Volmer equation. In general, Z_{TPB1} depends on the catalytic properties of the TPB and on the electrochemical conditions to which the TPB is subject, including p_{O_2}, c_e, c_v, $J_{o,TPB1}$, and the electrical potential difference across the TPB1 ($\Delta\phi$). Further, the Z_{TPB1} is influenced not only by the charge transfer across the TPB, but also by the mass transfer associated with the reaction in both solid and gas phases adjacent to the TPB. For instance, limited O_2 transport in the pores of MIEC may cause O_2 concentration polarization and thus contribute to Z_{TPB1}. Similarly, limited transport of defects in the solid MIEC adjacent to the TPB may also contribute to the Z_{TPB1}. The impedance to the transfer of ionic defects (such as $V_O^{\bullet\bullet}$) across the MIEC/el interface (excluding the TPB1), Z_{ii}, can be defined as

$$Z_{ii}(\omega) = \frac{\partial \eta_{ii}(\omega)}{\partial J_{ii}(\omega)} = f(c_i, \phi, J_{o,ii}, C_{ii}) \quad [3c]$$

where η_{ii}, J_{ii}, $J_{o,ii}$, and C_{ii} are, respectively, the overpotential across, the current density passing through, the exchange current density at, and the capacitance of the MIEC/el interface (excluding the TPB1). Similarly, Z_{ii} can be divided into two components: the impedance to charge transfer across the interface and the impedance to the mass transfer associated with the ion transfer in the vicinity of the interface.

Further, the kinetics of the interfacial reactions (Eq. 1b and 1c) are assumed to be finite in general. Accordingly, the defect concentrations at or near the MIEC/el or el/gas interface are influenced not only by thermodynamics but also by the kinetics of these reactions. Thus, significant interfacial polarizations due to charge and mass transfer are possible and the impedances to these processes, Z_{TPB1} and Z_{ii}, are expected to be a complex quality (containing real and imaginary components) in general.

In the region of the porous electrode ($0 < x < L$), the properties of the MIEC may vary with position. If the local resistivity (Ω cm), at a distance x away from the cc/MIEC interface, to transport of electrons and electron holes in the solid MIEC is $\rho_e(x)$, the total resistance to the transport of electrons and electron holes through the entire MIEC electrode of thickness, L, can be expressed as

$$R_{e,MIEC} = \int_0^L \rho_e(x)dx \quad [3d]$$

Similarly, if $\rho_i(x)$ is the local resistivity to transport of ionic defects in the MIEC, the total resistance to the transport of ionic defects through the entire MIEC is given by

$$R_{i,MIEC} = \int_0^L \rho_i(x)dx \quad [3e]$$

Because it is assumed that local charge neutrality is observed and bulk polarization is negligible in the bulk MIEC, the impedance of the bulk MIEC can be adequately approximated by resistance $R_{e,MIEC}$ and $R_{i,MIEC}$. When significant polarization occurs in the bulk phase of MIEC, $\rho_e(x)$ and $\rho_i(x)$ may no longer be pure resistive, as discussed in Appendix B.

The impedance of the MIEC/gas interface, however, should be a complex quality (frequency dependent) in general because the charge and mass transfer at or near the interface associated with the surface reaction may cause significant charge accumulation or depletion at the interface. If $\rho_r(x,\omega)$ represents the local surface resistivity (Ω cm) at an angular frequency ω to the reaction at the MIEC/gas interface, the impedance to the reaction at the entire MIEC/gas interface (Eq. 1f) and to the transport of the species involved in the surface reaction, $Z_{rt}(L,\omega)$, can be expressed as

$$\frac{1}{Z_{rt}(L,\omega)} = \frac{1}{\dfrac{\rho_r(0,\omega)}{(1-p)(1-\theta_{cc})} + \displaystyle\int_0^L \rho_i(x)dx} + \int_0^L \frac{dx}{-\left[\displaystyle\int_0^x \rho_e(t)dt\right]^2 / \rho_e(x) + \rho_r(x,\omega)/a(x) + \left[\displaystyle\int_x^L \rho_i(t)dt\right]^2 / \rho_i(x)} \quad [3f]$$

where θ_{cc} is the fraction of the MIEC surface at $x = 0$ covered by the current collector and $a(x)$ is the local surface area of the porous MIEC per unit volume (cm^2/cm^3), which characterizes the local microstructure of the MIEC electrode. The derivation of Eq. 3f is summarized in Appendix C. It is important to note that ρ_r is influenced not only by the surface catalytic properties of the MIEC but also by the associated mass transfer in the vicinity of the MIEC/gas interface. For instance, concentration polarizations in the gas phase or in the MIEC adjacent to the MIEC/gas interface may result in larger ρ_r at lower frequencies. In a steady state (i.e., $\omega \to 0$), however, ρ_r becomes real and Z_{rt} reduces to a steady-state resistance, $R_{rt} = \lim_{\omega \to 0} Z_{rt}$.

Equation 3f implies that the actual rate of the reaction at MIEC/gas interface is determined not only by the local surface properties, ρ_r, but also by the local microstructure, a, and the bulk transport properties of the MIEC, ρ_i and ρ_e. In fact, the bulk ionic transport, local surface reaction, bulk electronic transport, and the transport of O_2 in the pores of the MIEC are several consecutive steps necessary in order for reduction or evolution of O_2 gas to occur at the MIEC/gas interface. Accordingly, when the rate of any one step is sufficiently slow, the MIEC/gas interface is ineffective for the electrode reaction. The effectiveness of the MIEC/gas interface is characterized by $1/Z_{rt}$, which includes the impedance to surface reaction, to transport of defects in the MIEC, and to the transport of O_2 gas in the pores of the MIEC (which is lumped in ρ_r).

At the cc/MIEC interface at $x = 0$, the impedance to the electrochemical reaction at the TPB2, Z_{TPB2}, can be expressed as

$$Z_{TPB2}(\omega) = \frac{\partial \eta_{TPB2}(\omega)}{\partial J_{TPB2}(\omega)} = f(p_{O_2}, c_e, c_v, \phi, J_{o,TPB2}, C_{TPB2}) \quad [3g]$$

where η_{TPB2}, J_{TPB2}, $J_{o,TPB2}$, and C_{TPB2} are the overpotential across, the current density passing through, the exchange current density at, and the capacitance of the TPB2, respectively. The nature and the treatment of TPB2 are essentially the same as described for TPB1. The impedance to the electron transfer across the cc/MIEC interface (excluding the TPB2), Z_{ee}, is given by

$$Z_{ee}(\omega) = \frac{\partial \eta_{ee}(\omega)}{\partial J_{ee}(\omega)} = f(c_e, \phi, J_{o,ee}, C_{ee}) \quad [3h]$$

where η_{ee}, J_{ee}, $J_{o,ee}$, and C_{ee} are the overpotential across, the current density passing through, the exchange current density at, and the capacitance of the MIEC/el interface (excluding the TPB2), respectively. This interface can be considered as a typical metal/semiconductor interface and the $J_{ee} - \eta_{ee}$ relationship can be described using a diode equation.[18] The contribution of the MIEC/gas interface at $x = 0$ to electrode kinetics has been included in Eq. 3f.

Parallel Reaction Paths

The equivalent circuit shown in Fig. 4 clearly indicates that there are three parallel paths for oxygen reduction or evolution to occur in the cell

1. The reaction at the TPB1 (Eq. 1b), which requires transport of electronic defects to or away from the TPB1 through the MIEC and transport of O_2 to or away from the TPB1 through the pores of the MIEC, but does not require any transport of ionic defects through the MIEC electrode;
2. The reaction at the MIEC/gas interface (Eq. 1f), which requires simultaneous transport of both ionic and electronic defects to or away from the MIEC/gas interface through the MIEC and transport of O_2 to or away from the MIEC/gas interface through the pores of the MIEC; and
3. The reaction at the TPB2 (Eq. 1g), which requires transport of ionic defects to or away from the TPB2 through the MIEC and transport of O_2 gas to or away from the TPB2, but does not require any transport of electronic defects through the MIEC electrode.

The relative significance of each path depends critically on the transport (ρ_i and ρ_e) and the catalytic (ρ_r) properties of the MIEC electrode as well as the nature of the MIEC/el and cc/MIEC interfaces. The effect of O_2 transport in the pores of the MIEC on electrode kinetics is implicitly included in the interfacial impedance Z_{TPB1}, Z_{TPB2}, and ρ_r.

Clearly, oxygen transport in the MIEC and the reaction at the MIEC/gas interface are only part, not the entirety, of the electrode kinetics. Unlike liquid electrochemical system (with porous electrodes involving liquid electrolytes), TPBs in a solid-state system (with porous MIEC electrodes exposed to a gas) are the most important sites for electrode reactions. In general, the reactions occurring at least at one of the TPBs are an important part of the electrode kinetics and cannot be ignored without careful analysis and adequate justification. Consideration of at least one of the TPBs is a minimum requirement for any meaningful modeling of a solid-state system and failing to recognize TPBs as parallel paths to the MIEC/gas interface may result in erroneous conclusions.[9] For instance, in the absence of either ionic or electronic transport in the MIEC, electrode reaction may occur only at one of the TPBs.

Effect of Transport and Catalytic Properties of the MIEC

Limiting case I: zero ionic conduction.—In the limit of $\rho_i \to \infty$ (i.e., the electrode is, in fact, a pure electronic conductor such as Pt or Ag), $R_{i,MIEC} \to \infty$ and $Z_{rt} \to \infty$ and, hence, the reactions described by both Eq. 1f (the second path) and Eq. 1g (the third path) are unable to proceed. The only viable reaction path, then, is the first one, the reaction through the TPB1 described by Eq. 1b. Accordingly, the equivalent circuit shown in Fig. 4 reduces to the one shown in Fig. 5a. The total cell impedance, Z_{cell}, can then be expressed as

$$\frac{Z_{cell} - R_b}{2} = Z_{ee} + Z_{TPB1}; \qquad R_b = R_{i,el} + 2R_{e,MIEC} \quad [4a]$$

This equation is identical to Eq. C-5 in our earlier analysis,[9] which may reduce to

$$\frac{Z_{cell} - R_{i,el}}{2} \approx Z_{TPB1} \quad [4b]$$

since it is usually true that $Z_{ee} \ll Z_{TPB1}$ and $R_{e,MIEC} \ll R_{i,el}$ for cells with electrodes of good electronic conductors. This equation implies that the electrode kinetics and the cell impedance are dominated by the processes occurring at TPB1. In general, Z_{TPB1} may include two contributions, the impedance to charge transfer across the TPB1 and the impedance to the associated mass transfer in the vicinity of the TPB. The impedance to mass transfer is frequency-dependent and can be approximated by the Warburg impedance[19,20]

$$Z_W = R_{mt} \frac{\tanh \sqrt{j\omega t_W}}{\sqrt{j\omega t_W}} \quad [4c]$$

where R_{mt} represents the steady-state mass-transfer resistance (since $Z_W \to R_{mt}$ as $\omega \to 0$) and t_W corresponds to the time constant of the mass transport in the boundary layer adjacent to the interface. Clearly, the mass-transfer impedance vanishes at sufficiently high frequencies ($Z_W \to 0$ as $\omega \to \infty$) when the mass transport can no longer follow the changes in the applied perturbation.

Similarly, the impedance to charge transfer can be approximated by a resistance to charge transfer, R_{ct}, and an interfacial capacitance due to accumulation or depletion of charges at the TPB, C_{TPB1}, as schematically shown in Fig. 5b. If the Butler-Volmer equation is used to approximate the charge-transfer process, the R_{ct} can be defined as

$$R_{ct} = \lim_{J \to 0} \left(\frac{\partial \eta_{TPB1}}{\partial J_{TPB1}} \right) = \frac{RT}{F} \left(\frac{1}{\alpha_a + \alpha_c} \right) \frac{1}{J_{o,TPB1}} \quad [4d]$$

where α_a and α_c are the anodic and cathodic transfer coefficient, respectively, and $J_{o,TPB1}$ depends primarily on the

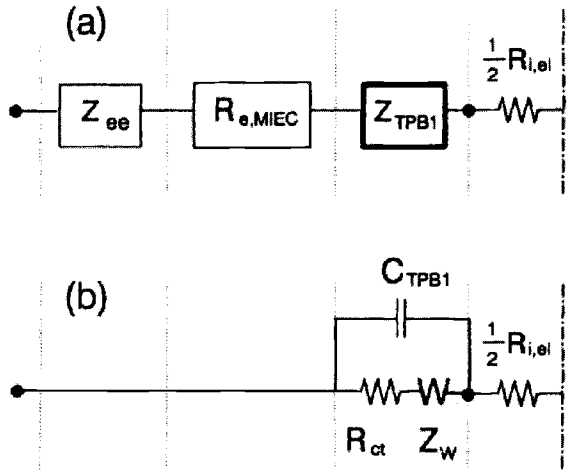

Fig. 5. (a) An equivalent circuit for a cell with electrodes of a pure electronic conductor and (b) an approximation to the circuit shown in (a) when Z_{ee} and $R_{e,MIEC}$ are sufficiently smaller than Z_{TPB1}. Further, the Z_{TPB1} is approximated by a capacitor, C_{TPB1}, in parallel to a charge-transfer resistance, R_{ct}, and a Warburg impedance, Z_W, of TPB1.

intrinsic catalytic activity of the TPB1, which is critically influenced by the properties of the MIEC and the electrolyte, including oxygen transport in the MIEC and surface catalytic properties.

Figure 6 shows several predicted spectra of the interfacial impedance, Z_{TPB1}, using the equivalent circuit shown in Fig. 5b and Eq. 4b and c. In Fig. 6a, the resistance to charge transfer is assumed to be comparable to the resistance to mass transfer ($R_{ct} = R_{mt}$) and the relaxation time constant for mass transfer is varied in orders of magnitude (from 0.01 to 100 s). The shapes of the interfacial impedance, Z_{TPB1}, are greatly influenced by the ratio of the time constant for mass transfer to that for charge transfer. In Fig. 6b, R_{mt} is assumed to dominate the interfacial impedance ($R_{mt} >> R_{ct}$) and, again, the time constant for mass transfer has dramatic effect on the shapes of Z_{TPB1}. In Fig. 6c, R_{ct} is assumed to dominate the interfacial impedance ($R_{ct} >> R_{mt}$) and the shapes of Z_{TPB1} are determined primarily by the charge-transfer process. The predicted spectra indicate that the equivalent circuits and derived equations can be used to interpret the impedance response of a cell with electrodes of a pure electronic conductor (such as Pt or Ag). Further, they can be used to approximate the impedance response of a cell with MIEC electrodes of infinite thickness and high electronic conductivity, when the rate of oxygen diffusion in the MIEC or the surface reaction rate is much slower than any other processes occurring in the cell, as described elsewhere.[9]

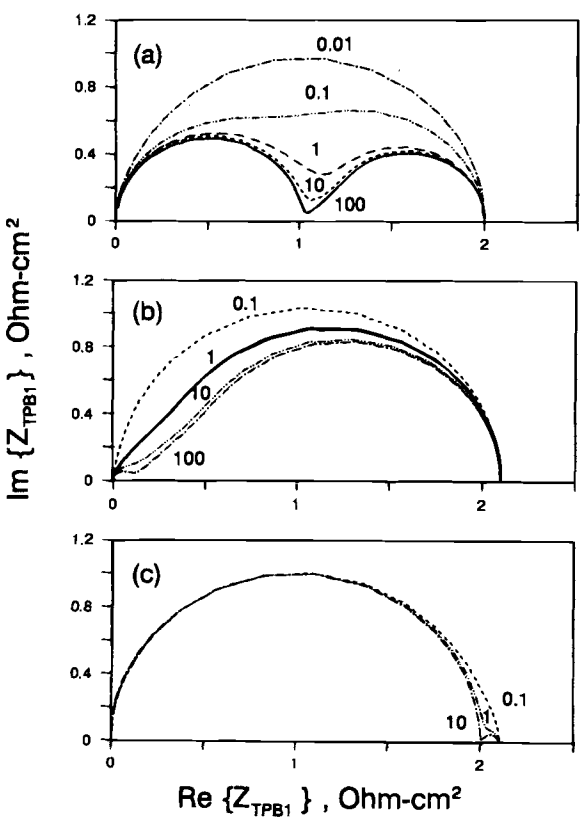

Fig. 6. Predicted frequency dependence of interfacial impedance, Z_{TPB1}, using the circuit shown in Fig 5b and Eq. 4c for Z_W. The number by each impedance spectrum represents the time constant for mass transfer in seconds. The parameters used in the calculation were $R_{ct} = R_{mt} = 1.0\ \Omega\ cm^2$, $C_{TPB1} = 0.01\ F/cm^2$, and $t_W = 0.01$, 0.1, 1, 10, and 100 s in (a); $R_{ct} = 0.1\ \Omega\ cm^2$, $R_{mt} = 1.0\ \Omega\ cm^2$, $C_{TPB1} = 0.1\ F/cm^2$, and $t_W = 0.1$, 1, 10, and 100 s in (b); $R_{mt} = 0.1\ \Omega\ cm^2$, $R_{ct} = 1.0\ \Omega\ cm^2$, $C_{TPB1} = 0.01\ F/cm^2$, and $t_W = 0.1$, 1, 10, and 100 s in (c).

Limiting case II: zero electronic conduction.—In the limit of $\rho_e \rightarrow \infty$ (i.e., the electrode is, in fact, a pure ionic conductor), $R_{e,MIEC} \rightarrow \infty$ and $Z_{rt} \rightarrow \infty$ and, hence, the reaction through either the first path (Eq. 1b) or the second path (Eq. 1f) is unable to proceed. The only possible reaction path, then, is the third one, the reaction through the TPB2 described by Eq. 1g. The total cell impedance can then be approximated by

$$Z_{cell} \approx R_b + 2[Z_{ii} + Z_{TPB2}], \qquad R_b = R_{i,el} + 2R_{i,MIEC} \qquad [5]$$

Obviously, the porous electrode with $\rho_e \rightarrow \infty$ is unable to function as an electrode; it acts only as an extension of the electrolyte because of the lack of electronic transport. As a result, the electrode kinetics is dominated by the processes occurring at TPB2. Again, both charge and mass transfer at or near the TPB2 may significantly influence the electrode kinetics and hence cell impedance. The treatment of TPB2 is similar to that of TPB1 as discussed earlier.

Limiting case III: zero catalytic activity.—In the limit of $\rho_r \rightarrow \infty$, $Z_{rt} \rightarrow \infty$ and, hence, the reaction described by Eq. 1f (the second path) is still unable to proceed, or the MIEC/gas interface is still inactive. The cell impedance can be expressed as

$$Z_{cell} = R_{i,el} + 2\left[\frac{(Z_{TPB1} + R_{e,MIEC} + Z_{ee})(Z_{ii} + R_{i,MIEC} + Z_{TPB2})}{(Z_{TPB1} + R_{e,MIEC} + Z_{ee}) + (Z_{ii} + R_{i,MIEC} + Z_{TPB2})}\right] \qquad [6a]$$

which may be approximated by

$$Z_{cell} \approx R_{i,el} + 2\left[\frac{(Z_{TPB1})(Z_{TPB2})}{Z_{TPB1} + Z_{TPB2}}\right] \qquad [6b]$$

if the MIEC is sufficiently conductive both ionically and electronically so that $(R_{e,MIEC} + Z_{ee}) << Z_{TPB1}$ and $(R_{i,MIEC} + Z_{ii}) << Z_{TPB2}$. Under these conditions, the electrode kinetics and cell impedance are controlled by TPB1 and TPB2.

The representative case.—The most important class of MIECs for electrode applications are those which have overwhelming electronic conductivity, i.e., $\rho_e << \rho_i$, but with finite rate of ionic transport and finite rate of surface reaction (ρ_r and ρ_i are finite). Under this condition, $R_{e,MIEC}$ in the circuit may be neglected since $R_{e,MIEC} << Z_{TPB1}$. In order to simplify the circuit further, one may increase the thickness of the porous MIEC until $R_{i,MIEC} >> Z_{TPB1}$ and $R_{i,MIEC} >> Z_{rt}$ so that the reaction through the third path (Eq. 1g) may be neglected. Under these conditions, the equivalent circuit in Fig. 4 can be adequately approximated by the ones shown in Fig. 7. Thus, the impedance of the cell can be approximated by

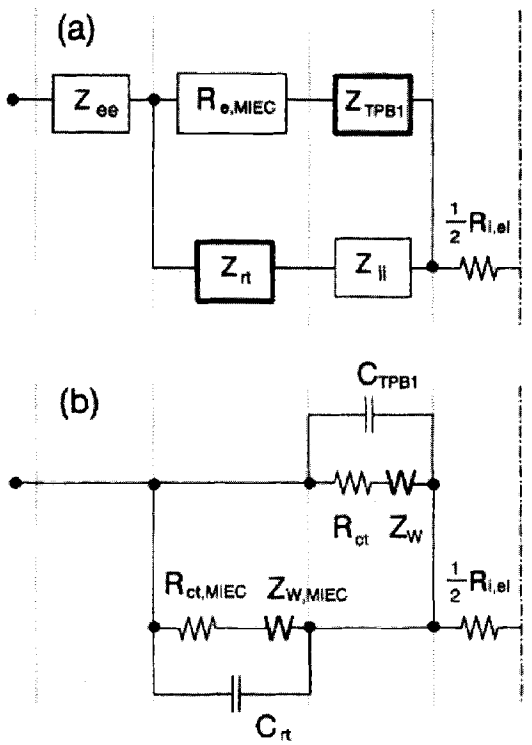

Fig. 7. (a) An equivalent circuit for a cell with electrodes of a porous MIEC of infinite thickness and (b) an approximation to the circuit shown in (a) when Z_{ee}, $R_{e,MIEC}$, and Z_{ii} are negligible. Further, similar to the approximation made to Z_{TPB1} in Fig. 5, the Z_{rt} is approximated by a capacitor, C_{rt}, in parallel to a charge-transfer resistance, $R_{ct,MIEC}$, and a Warburg impedance, $Z_{W,MIEC}$, where $R_{rt} = R_{ct,MIEC} + \lim_{[\omega \to 0]} Z_{W,MIEC}$.

$$Z_{cell} = R_{i,el} + 2\left[Z_{ee} + \frac{Z_{TPB1}(Z_{rt} + Z_{ii})}{Z_{TPB1} + (Z_{rt} + Z_{ii})}\right] \quad [7a]$$

This is the expression for the impedance of a cell with two identical MIEC electrodes of infinite thickness and sufficiently high electronic conductivity. Since the interfacial impedance, Z_{ee}, is typically small under the assumptions (particularly when the contact between the MIEC and the current collector is made ohmic, which can be accomplished by tailoring the Fermi levels of the two materials), Eq. 7a simplifies to

$$\frac{Z_{cell} - R_{i,el}}{2} \approx \frac{Z_{TPB1}}{1 + \frac{Z_{TPB1}}{Z_{rt} + Z_{ii}}} = \frac{Z_{rt} + Z_{ii}}{1 + \frac{Z_{rt} + Z_{ii}}{Z_{TPB1}}} \quad [7b]$$

Equations 7a and 7b as well as the equivalent circuit shown in Fig. 7 imply that the oxygen reduction or evolution has two parallel paths. One path is the direct electrochemical reaction at the TPB1 at $x = L$ while the other path is the MIEC/gas interface. The second path involves several sequential steps: transfer of ionic defects across the MIEC/el interface (Z_{ii}), transport of ionic defects to or away from the MIEC/el interface through the MIEC (ρ_i), and the kinetics of the reaction at MIEC/gas interface (ρ_r) which may also be influenced by the O_2 transport in the pores. Similar to the approximation made to Z_{TPB1} shown in Fig. 5b, the circuit element characterizing the effectiveness of the MIEC/gas interface, Z_{rt}, may also be approximated by a proper combination of a charge-transfer resistance ($R_{ct,MIEC}$), a capacitance (C_{rt}), and a Warburg impedance to mass transfer ($Z_{W,MIEC}$), as shown in Fig. 7b.

When the impedance of one path is much greater than that of the other path, Eq. 7b can be simplified further.

1. The first path (TPB1) dominating.—When $Z_{TPB1} << (Z_{rt} + Z_{ii})$, e.g., when the interfacial impedance Z_{TPB1} is sufficiently smaller than the impedance of the MIEC, Z_{rt}, Eq. 7b reduces to Eq. 4b. In other words, Eq. 4b (or Eq. C-5 in Ref. 9) defines the impedance of a cell with porous MIEC electrodes of infinite thickness when Z_{TPB1} is sufficiently smaller than the impedance of any one of the following processes occurring in the cell: the transfer of ionic defects across the MIEC/el interface, the transport of ionic defects in the MIEC, or the kinetics of the reaction at the MIEC/gas interface (including the associated mass transfer in both solid and gas phases). Accordingly, the impedance of the cell is primarily determined by the impedance to the reaction at TPB1 (including associated mass transfer processes) while neither Z_{rt} nor Z_{ii} is observable in an impedance measurement.[9] The MIEC/gas interface is practically inactive. Any effect of the MIEC on electrode kinetics must be due to the influence of the MIEC on the catalytic property of the TPB1.

2. The second path dominating.—When the processes occurring at or near the TPB1 are completely ignored (i.e., assuming that $Z_{TPB1} \to \infty$), Eq. 7b reduces to

$$\frac{Z_{cell} - R_{i,el}}{2} \approx Z_{rt} + Z_{ii} \quad [8a]$$

Under these conditions, naturally, the impedance of the cell is determined only by Z_{rt} and Z_{ii} while Z_{TPB1} is not observable in an impedance measurement. Further, when Z_{ii} is completely ignored (i.e., assuming that $Z_{ii} \to 0$), Eq. 8a reduces to

$$\frac{Z_{cell} - R_{i,el}}{2} \approx Z_{rt} \quad [8b]$$

This equation implies that the impedance of the cell is dominated by the reactions at the MIEC/gas interface and the transport of defects in the MIEC (if the transport of O_2 in the pores is sufficiently fast). However, this does not represent a general case or "a more complex version" as claimed by Adler et al.[7]; it represents, at best, an unrealistic case where the electrolyte-electrode interface is completely ignored. In fact, it is a consequence of failing to recognize TPBs as parallel paths to the MIEC/gas interface and failing to appreciate the significance of TPBs in solid-state systems.[9] In general, Eq. 7a should be used to describe the impedance of a cell with MIEC electrodes of infinite thickness ($L \to \infty$) and uniform Fermi level ($\rho_e \to 0$).

Effect of Electrode Thickness (L)

The effectiveness of the MIEC/gas interface of a porous MIEC electrode, characterized by Z_{rt}, is determined not only by the transport and catalytic properties of the MIEC but also by the thickness of the MIEC, as implied by Eq. 3f. In order to estimate the effect of L on Z_{rt}, it is assumed in the following discussion that ρ_e, ρ_i, ρ_r, and a are relatively uniform throughout the thickness of the MIEC (or consider them to be the average values over the thickness of the MIEC electrode). Under this assumption, Eq. 3f reduces to

$$\frac{1}{Z_{rt}(L)} = G_s(L) + G_{rt}(L) \quad [9a]$$

where

$$G_s(L) = \frac{1}{\frac{\rho_r}{(1-p)(1-\theta_{cc})} + \rho_i L} \quad [9b]$$

$$G_{rt}(L) = \int_0^L \frac{dx}{-\rho_e x^2 + \rho_r/a + \rho_i(L-x)^2} \quad [9c]$$

Clearly, the G_s represents the contribution from the surface (or MIEC/gas interface) at $x = 0$ of the MIEC electrode. While the effect of L on G_s is apparent as implied by

Eq. 9b, the dependence of G_{rt} on L is complex and further analysis is necessary in order to gain some insight. In particular, G_s diminishes as $\theta_{cc} \rightarrow 1$ and as ρ_i or L increases. When $\rho_i >> \rho_e$ or L is sufficiently large, in fact, G_s is negligible and $1/Z_{rt} \approx G_{rt}$. Thus, in the following discussions, we focus only on the effect of L on G_{rt}.

Depending on the relative values of ρ_i and ρ_e, integration of Eq. 9c may result in different expressions for $G_{rt}(L)$. Since the most representative MIECs for electrode applications are those with overwhelming electronic conductivity, the case with $\rho_i > \rho_e$ is discussed here in detail while the other two cases, $\rho_e > \rho_i$ and $\rho_i = \rho_e$, are briefly summarized in Appendix D.

Integrating Eq. 9c under the condition of $\rho_i > \rho_e$, we find that $G_{rt}(L)$ is given by

$$G_{rt}(L) = \frac{1}{\sqrt{f(L)}} \arctan\left[\frac{L\sqrt{f(L)}}{\rho_r/a}\right], \quad 0 \le L < \sqrt{\frac{\rho_r}{a}\left(\frac{\rho_i - \rho_e}{\rho_i\rho_e}\right)} \qquad [10a]$$

$$= \frac{1}{2\sqrt{-f(L)}} \ln\left[\frac{\rho_r/a + L\sqrt{-f(L)}}{\rho_r/a - L\sqrt{-f(L)}}\right]$$

$$\sqrt{\frac{\rho_r}{a}\left(\frac{\rho_i - \rho_e}{\rho_i\rho_e}\right)} < L < \sqrt{\frac{\rho_r}{a}\left[\frac{\rho_i - \rho_e}{2\rho_i\rho_e} + \sqrt{\left(\frac{\rho_i - \rho_e}{2\rho_i\rho_e}\right)^2 + \frac{1}{\rho_i\rho_e}}\right]} \qquad [10b]$$

$$= \sqrt{\frac{(\rho_i - \rho_e)/\rho_i\rho_e}{\rho_r/a}}, \qquad L = \sqrt{\frac{\rho_r}{a}\left(\frac{\rho_i - \rho_e}{\rho_i\rho_e}\right)} \qquad [10c]$$

where

$$f(L) = \frac{\rho_r}{a}(\rho_i - \rho_e) - \rho_i\rho_e L^2, \qquad \rho_i > \rho_e \qquad [11]$$

Differentiating Eq. 10a and b with respect to L, we find that the variation in $G_{rt}(L)$ with L in each range of L can be expressed, respectively, as

$$\frac{\partial}{\partial L}[G_{rt}(L)] = \frac{\rho_i\rho_e L}{[f(L)]^{3/2}} \arctan\left[\frac{L\sqrt{f(L)}}{\rho_r/a}\right] + \frac{(\rho_r/a)[1 - \rho_i\rho_e L^2/f(L)]}{(\rho_r/a)^2 + L^2 f(L)} \qquad [12a]$$

$$= \frac{-\rho_i\rho_e L}{[-f(L)]^{3/2}} \ln\left[\frac{\rho_r/a + L\sqrt{-f(L)}}{\rho_r/a - L\sqrt{-f(L)}}\right] + \frac{(\rho_r/a)[1 - \rho_i\rho_e L^2/f(L)]}{(\rho_r/a)^2 + L^2 f(L)} \qquad [12b]$$

From a practical point of view, however, most MIECs for electrode applications satisfy the condition of $L < \sqrt{(\rho_r/a)(\rho_i - \rho_e/\rho_i\rho_e)}$. Accordingly, Eq. 10a and 12a may be adequate for most MIECs with $\rho_i > \rho_e$. In the limit of $\rho_e \rightarrow 0$ (or $\rho_e << \rho_i$ and $\rho_e L^2 << \rho_r/a$), Eq. 10 and 12 reduce, respectively, to

$$G_{rt}(L) = \frac{1}{\sqrt{\rho_i\rho_r/a}} \arctan\left(\frac{L\sqrt{\rho_i}}{\sqrt{\rho_r/a}}\right) \qquad [13]$$

$$\frac{\partial G_{rt}(L)}{\partial L} = \frac{1}{\rho_r/a + \rho_i L^2} \qquad [14]$$

Evaluation of Eq. 13 indicates that $G_{rt}(L)$, the effectiveness of the MIEC/gas interface for the electrode reaction, increases monotonically with thickness, L, and approaches a maximum as $L \rightarrow \infty$ [note that $G_{rt}(L)$ is an arctan function of L]. Evaluating Eq. 14, however, we find that, $\partial G_{rt}/\partial L$, the rate of increase in $G_{rt}(L)$ with L, decreases rapidly with L. Beyond certain thickness, increasing L is ineffective in improving $G_{rt}(L)$. If a characteristic thickness, L_c, is defined as

$$G_{rt}(L_c) = \frac{G_{rt}(\infty)}{2} \qquad [15]$$

where $G_{rt}(\infty)$ represents the G_{rt} of a porous MIEC electrode of infinite thickness, then L_c is given by

$$L_c = \sqrt{\frac{\rho_r/a}{\rho_i}} \qquad [16]$$

Thus, the characteristic thickness is determined by the ratio of the surface resistivity normalized by the surface area, ρ_r/a, to the ionic resistivity, ρ_i. Equation 16 is similar to the expression derived by Abeles et al.[4,21] to describe the width of the chemically active zone of a porous electrode applied to a dense MIEC membrane. In Fig. 8, normalized G_{rt}, $G_{rt}(L/L_c)/G_{rt}(\infty)$, and normalized variation in G_{rt} with thickness, $(\rho_r/a)\partial G_{rt}(L)/\partial L$, are plotted as a function of normalized thickness, L/L_c. The thickness of the electrochemically active layer of a porous MIEC electrode, δ, is only a few times of the characteristic thickness, L_c; when $L > \delta$, increasing the thickness of the electrode has little influence on G_{rt}.

Similarly, for MIECs with $\rho_i > \rho_e \neq 0$ and $L << \sqrt{(\rho_r/a)(\rho_i - \rho_e/\rho_i\rho_e)}$, a characteristic thickness L_c can be estimated from

$$L_c^2 = \frac{\rho_r}{a}\left[\frac{\rho_i - \rho_e}{2\rho_i\rho_e} - \sqrt{\left(\frac{\rho_i - \rho_e}{2\rho_i\rho_e}\right)^2 - \frac{1}{\rho_i\rho_e}}\right] \rightarrow \left(\frac{\rho_r/a}{\rho_i}\right) \text{ when } \rho_i >> \rho_e \qquad [17]$$

Equations 16 and 17 can be used to estimate the useful thickness, δ, of a porous MIEC electrode.

Figure 9 shows the effect of the properties and microstructure of a porous MIEC electrode on $G_{rt}(L)$, $\partial G_{rt}/\partial L$, and L_c of the MIEC electrode, as calculated using Eq. 10a, 12a, and 17. It can be seen that, when the ionic transport is much slower than the surface reaction and electronic transport (i.e., $\rho_r/a << \rho_i L^2$ and $\rho_e << \rho_i$), the effectiveness of the MIEC/gas interface is determined primarily by ρ_i. The larger the ρ_i, the thinner the L_c and the electrochemically active layer, δ. Similarly, as the surface reaction gets faster (i.e., ρ_r/a or the ratio of $(\rho_r/a)/\rho_i$ gets smaller), L_c and δ become smaller. On the other hand, however, when the

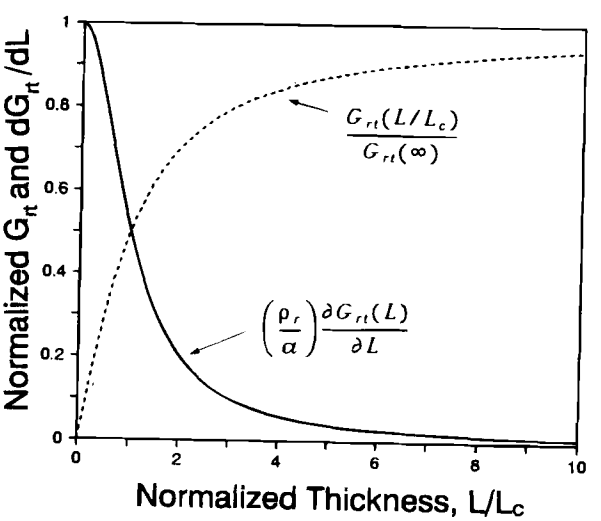

Fig. 8. Normalized G_{rt} and variation in G_{rt} with thickness for a porous MIEC with $\rho_e \rightarrow 0$, as predicted using Eq. 13 and 14.

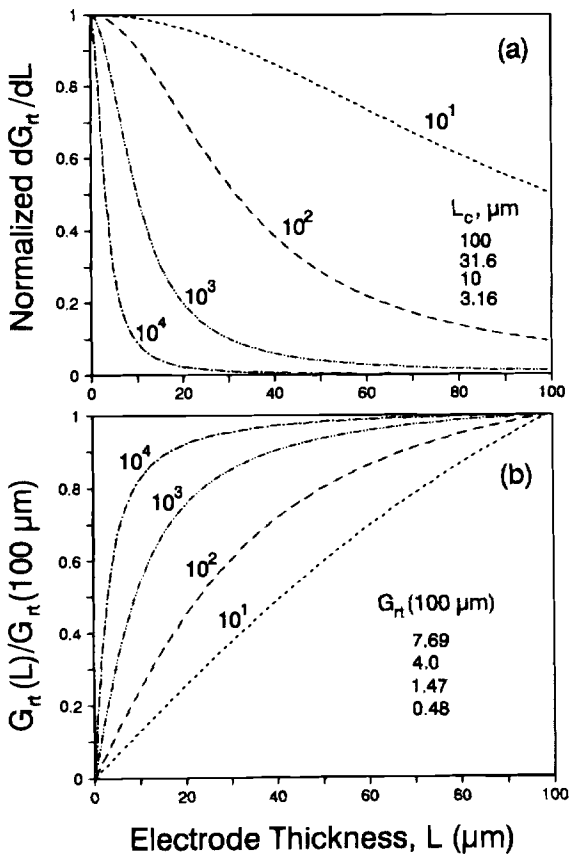

Fig. 9. Effect of transport and surface properties of a porous MIEC on G_{rt} and $\partial G_{rt}/\partial L$, as predicted using Eq. 10a and 12a, respectively. The number by each curve represents ρ_i in ohms centimeter and other assumed values were $\rho_r/a = 10^{-3}\ \Omega\ cm^3$ and $\rho_e = 10^{-3}\ \Omega$ cm. The numbers next to L_c in (a) are the characteristic thickness in microns while the numbers next to G_{rt} (100 μm) in (b) are the values of G_{rt} in $\Omega^{-1}\ cm^{-2}$ for the electrode with thickness of 100 μm corresponding to $\rho_i = 10^1, 10^2, 10^3$, and 10^4, respectively.

ionic transport is sufficiently fast or the surface reaction is sufficiently slow [i.e., the ratio $(\rho_r/a)/\rho_i$ is sufficiently large], $G_{rt}(L)$ increases linearly with the thickness of the MIEC, indicating that increase in thickness improves the effectiveness of the MIEC/gas interface. In the limit of $\rho_i \to 0$ and $\rho_e \to 0$, i.e., the transport of both ionic and electronic defects in the MIEC are much faster than the rate of surface reaction, the thicker the MIEC, the greater the $G_{rt}(L)$ for a given ρ_r/a, simply because a thicker MIEC has more MIEC/gas interface area available for the reaction to take place. Under this condition, the entire MIEC/gas interface is electrochemically active for the electrode reactions.

Finally, it is important to recognize that the effect of electrode thickness on electrode kinetics is important only when the reaction passing through the MIEC/gas interface is significant. The relative significance of each path is influenced by the properties of the MIEC as well as the MIEC/el and cc/MIEC interface (including the TPBs). When $Z_{TPB1} << Z_{ii}$ or $Z_{TPB1} << Z_{rt}$, for instance, the reaction passing through the MIEC/gas interface is insignificant; the electrode kinetics are dominated by the TPBs and largely independent of electrode thickness. Under this condition, L_c or δ has no practical significance.

Conclusions

Equivalent circuit analyses indicate that, in general, there are three parallel paths for reduction or evolution of oxygen in a cell with porous MIEC electrodes: (*i*) the reaction at the TPB between the electrolyte, the MIEC, and the gas phase, (*ii*) the reaction at the MIEC/gas interface, and (*iii*) the reaction at the TPB between the MIEC, the current collector, and the gas. The relative significance of each path is determined not only by the transport and catalytic properties of the MIEC electrode but also by the nature of the interfaces between the MIEC and other cell components (such as electrolyte and current collector). In general, the interfacial processes cannot be ignored without careful analysis and adequate justification and it is improper to state that oxygen diffusion in the MIEC electrode and the reaction at the MIEC/gas interface are the only processes that dominate the electrode kinetics of a cell with porous MIEC electrodes. In the absences of ionic transport in the MIEC, for instance, only the reaction at TPB1 may occur while in the absence of electronic transport in the MIEC, only the reaction at TPB2 may occur. Accordingly, failing to recognize TPBs as parallel paths to the MIEC/gas interface may result in erroneous conclusions.

The effectiveness of the MIEC/gas interface of a porous MIEC electrode is characterized by, Z_{rt}, which is determined by the rates of several sequential processes necessary for the surface reaction to occur, including simultaneous transport of ionic and electronic defects in the MIEC, reaction at the MIEC/gas interface, and the transport of O_2 in the pores of the MIEC.

Further, as a first-order approximation, it is demonstrated that the thickness of the electrochemically active layer of a porous MIEC electrode, δ, varies dramatically with the properties of the MIEC and the nature of the interfaces. In general, δ decreases with the increased rate of surface reaction and with decreased transport of ionic or electronic defects in the MIEC. In the absence of ionic or electronic transport, for instance, the δ approaches zero, implying that oxygen reduction or evolution can occur only at TPB1 or TPB2. When the rate of ionic and electronic transport is much faster than the rate of the surface reaction, on the other hand, the thicker the electrode, the smaller the Z_{rt} because more surface area becomes available for the reaction at the MIEC/gas interface to occur. Under this condition, the entire MIEC/gas interface is active for electrode reaction.

Acknowledgment

The author would like to acknowledge Dr. Benjamin Abeles and Professor Jack Winnick for their careful review of this manuscript and for their valuable suggestions. This work was supported by NSF (Award No. DMR-9357520) and EPRI (Contract No. RP 1676-19) and their financial support of this research is gratefully acknowledged.

Manuscript submitted April 10, 1997; revised manuscript received July 25, 1997.

Georgia Institute of Technology assisted in meeting the publication costs of this article.

APPENDIX A

Cells with a Mixed Conducting Electrolyte

When the electronic transference number of the electrolyte in the cell shown in Fig. 1 is not negligible, the electrolyte must be treated as an MIEC. If the mixed conducting electrolyte is dense and homogeneous so that neither electrochemical reaction nor space-charge polarization occur significantly within the dense electrolyte, the electrochemical behavior of the cell can be adequately approximated by the circuit shown in Fig. A-1. Compared to the circuit shown in Fig. 4, two additional circuit elements are introduced. One element is $R_{e,el}$, the resistance to the motion of electronic defects in the dense electrolyte, which can be defined as

$$R_{e,el} = L_{el}/\sigma_{e,el} \qquad [A\text{-}1]$$

where $\sigma_{e,el}$ is the electronic conductivity of the electrolyte. The other element is Z_{eel}, the impedance to electron transfer across the MIEC/el interface. The nature and the treatment of Z_{eel} should be similar to those of Z_{ee} discussed earlier. The equivalent circuit shown in Fig. A-1 may also be used to approximate the electrochemical behavior of a dense MIEC membrane with a porous MIEC layer on surfaces for gas separation or electrocatalysis.[3-6]

When the electronic conductivity is much greater than the ionic conductivity in both the dense MIEC electrolyte

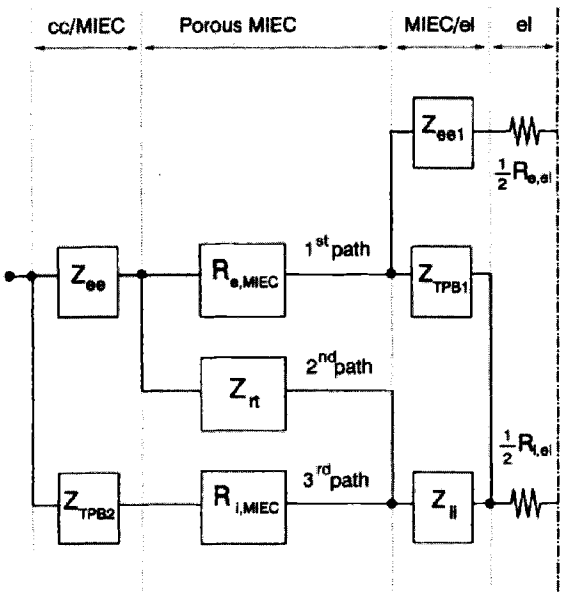

Fig. A-1. An equivalent circuit for a solid-state cell with a mixed conducting electrolyte (el, $0 < t_e < 1$), two porous electrodes of an MIEC ($0 < t_e < 1$), and two current collectors (cc, $t_e = 1$) under the influence of a small ac perturbation.

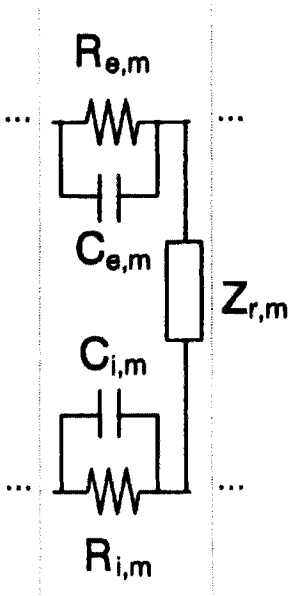

Fig. B-1. An equivalent circuit for an arbitrary element m ($1 \leq m \leq n$) of the MIEC electrode when the bulk polarization in the MIEC is no longer negligible. The $R_{e,m}$, $R_{i,m}$, and $Z_{r,m}$ are the same as defined in Fig. 4 and $C_{e,m}$ and $C_{i,m}$ represent the capacitance due to polarization of electronic and ionic defects, respectively, in the bulk phase of element m.

and the porous MIEC electrodes, the cell impedance can be approximated by

$$\frac{Z_{cell} - R_b}{2} = Z_{ee} + Z_{eel} \qquad [A\text{-}2]$$

where R_b represents the "bulk resistance" of the cell and can be expressed as

$$R_b = R_{e,el} + 2R_{e,MIEC} \qquad [A\text{-}3]$$

Further, when the dense electrolyte and porous electrodes are made of the same MIEC, impedance Z_{ee1} at the MIEC/el interface may be neglected. Thus, Z_{ee} and $R_{e,MIEC}$ may be determined from impedance measurements of a cell with configuration of

p_{O_2}, cc/porous MIEC/dense MIEC/porous MIEC/cc, p_{O_2}

This cell can be used to determine the contact resistance between the cc and MIEC electrode, Z_{ee}, and the electronic resistance of the MIEC electrode, $R_{e,MIEC}$.

APPENDIX B

Composite MIEC Electrodes and Bulk Polarization

When the porous MIEC electrode in the cell shown in Fig. 1 is a composite MIEC consisting of two or more phases,[11] the equivalent circuit (Fig. 4) for approximation of the electrochemical behavior of such a cell will remain the same as long as the space-charge polarization within the solid phase of the MIEC is assumed to be insignificant. However, the electrochemical processes occurring in the porous electrode are different. For instance, the reaction at the MIEC/gas interface can no longer be described using Eq. 1f; the proper reaction should be written as

$$V_O^{\bullet\bullet}(ic) + 2e'(ec) + \frac{1}{2}O_2(gas) = O_O^{\times}(ic) \qquad [B\text{-}1]$$

where ic and ec represent, respectively, the ionically conductive and the electronically conductive phase of the composite MIEC electrode. Accordingly, the active sites for electrode reactions at the MIEC/gas interface are, in fact, the TPB between the ic, the ec, and O_2 gas. The nature and the treatment of the TPB at the MIEC/gas interface should be similar to those of the TPBs at the MIEC/el and cc/MIEC interfaces discussed earlier.

If the polarization processes are extended to the bulk of the MIEC, not confined to the MIEC/gas interface, the assumption of local charge neutrality in the MIEC may no longer be valid; the displacement current induced in the bulk phase of the MIEC, when a time-dependent electric field is applied, may become significant. Under these conditions, the impedance to the motion of ionic and electronic defects in the MIEC can no longer be adequately approximated by a pure resistance; the $R_{e,MIEC}$ and $R_{i,MIEC}$ as defined by Eq. 3d and 3e should be a complex quality because ρ_e and ρ_i are no longer pure resistive. In this case, the electrochemical behavior of an arbitrary element $m (1 \leq m \leq n)$ of the MIEC electrode can be approximated by the equivalent circuit shown in Fig. B-1. Compared to the circuit shown in Fig. 4a, two capacitances, $C_{e,m}$ and $C_{i,m}$, are added to element m in order to take into consideration the polarization of, respectively, electronic and ionic defects in the bulk of the MIEC.

In general, the local specific impedance (Ω cm) at an angular frequency ω to the motion of defect k in an MIEC can be expressed as

$$\rho_k(x,\omega) \equiv \frac{1}{z_k F}\left[\frac{\partial \nabla \tilde{\mu}_k(x,\omega)}{\partial J_k(x,\omega)}\right] \qquad [B\text{-}2]$$

Thus, the specific impedance to the motion of electronic and ionic defects can then be expressed, respectively, as

$$\frac{1}{\rho_e(x,\omega)} = \sum_k \left(\frac{1}{\rho_k(x,\omega)}\right), \quad k = \text{electron defects} \qquad [B\text{-}3a]$$

$$\frac{1}{\rho_i(x,\omega)} = \sum_k \left(\frac{1}{\rho_k(x,\omega)}\right), \quad k = \text{ionic defects} \qquad [B\text{-}3b]$$

In a steady state ($\omega \to 0$) or in the absence of significant bulk polarization (i.e., $\nabla c_k \approx 0$), Eq. B-3a and B-3b reduce, respectively, to

$$\rho_e(x) \approx \frac{1}{F^2[u_e c_e(x) + u_h c_h(x)]} \qquad [B\text{-}4a]$$

$$\rho_i(x) \approx \frac{1}{\sum_k z_k^2 F^2 u_k c_k(x)}, \quad k = \text{ionic defects} \qquad [B\text{-}4b]$$

APPENDIX C

Transmission Line Model and Derivation of Eq. 3f

Imagine that the MIEC electrode of thickness L is sliced into n layers, each with thickness of L/n. If $R_{e,m}$, $R_{i,m}$, and $Z_{r,m}$ represent the impedance to electronic transport, ionic transport, and the impedance to the reaction at the MIEC/gas interface of a single layer m (where $1 \leq m \leq n$), the electrochemical behavior of the cell can be approximated by a discretized form of a transmission line model as schematically shown in Fig. 4a. In the absence of bulk polarization, $R_{e,m}$ and $R_{i,m}$ may be considered to be real while $Z_{r,m}$ should be treated as a complex quality in general due to interfacial polarization.

Consider an arbitrary element m ($1 \leq m \leq n$) of the MIEC electrode. The reaction at the MIEC/gas interface (described by Eq. 1f) of element m requires that $V_O^{\bullet\bullet}$ ions transport from the electrolyte to the element m, electrons (e') move from the cc to the element, and O_2 gas move to the element m through the pores of the MIEC. The impedance to the motion of electronic defects through the MIEC from the cc to the element m (or from the element m to the cc) can be expressed as

$$\sum_{l=1}^{l=m} R_{e,l} = \sum_{l=1}^{l=m} \rho_{e,l}\left(\frac{L}{n}\right) \qquad [C\text{-}1a]$$

Similarly, the impedance to the motion of ionic defects through the MIEC from the electrolyte to the element m (or from the element m to the electrolyte) is given by

$$\sum_{l=m+1}^{l=n} R_{i,l} = \sum_{l=m+1}^{l=n} \rho_{i,l}\left(\frac{L}{n}\right) \qquad [C\text{-}1b]$$

While the impedance at an angular frequency ω to the reaction at the MIEC/gas interface of element m can be expressed as

$$Z_{r,m}(\omega) = \frac{\rho_{r,m}(\omega)}{a_m\left(\frac{L}{n}\right)} \qquad [C\text{-}1c]$$

where the frequency-dependent $\rho_{r,m}$ includes the impedance to the charge-transfer at the interface and the impedance to the associated mass-transfer near the interface of element m. The a_m represents the specific area of the element, i.e., the ratio of the MIEC/gas interface area to the volume of element m. Further, if the surface of the porous MIEC at $x = 0$ is not completely covered by the current collector (cc), the impedance to the reaction at this surface (or MIEC/gas interface at $x = 0$) can be expressed as

$$Z_{r,s}(\omega) = \frac{\rho_{r,s}(\omega)}{(1-p)(1-\theta_{cc})} \qquad [C\text{-}1d]$$

where p is the porosity of the MIEC and θ_{cc} is the fraction of the MIEC surface at $x = 0$ covered by the current collector.

The impedance to the reaction at the MIEC/gas interface of the element m and to the transport of the species involved in the reaction, $Z_{rt,m}(\omega)$, can be expressed as

$$Z_{rt,m}(\omega) = \sum_{l=1}^{l=m} R_{e,l} + Z_{r,m}(\omega) + \sum_{l=m+1}^{l=n} R_{i,l} \qquad [C\text{-}2a]$$

Similarly, the impedance to the reaction at the MIEC/gas interface at $x = 0$ and to the transport of the species involved in the reaction, $Z_{rt,s}(\omega)$, can be expressed as

$$Z_{rt,s}(\omega) = \frac{\rho_{r,s}(\omega)}{(1-p)(1-\theta_{cc})} + \sum_{l=1}^{l=n} R_{i,l} \qquad [C\text{-}2b]$$

Accordingly, summation of $Z_{rt,m}(\omega)$ over all elements (from $m = 1$ to $m = n$), together with $Z_{rt,s}$, results in $Z_{rt}(L, \omega)$, the total impedance to the reaction at the entire MIEC/gas interface (of a porous MIEC electrode of thickness L) and to the transport of the species involved in the surface reaction

$$\frac{1}{Z_{rt}(L,\omega)} = \frac{1}{Z_{rt,s}(\omega)} + \sum_{m=1}^{m=n}\left[\frac{1}{Z_{rt,m}(\omega)}\right]$$

$$= \frac{1}{\frac{\rho_{r,s}(\omega)}{(1-p)(1-\theta_{cc})} + \sum_{l=1}^{l=n} \rho_{i,l}\left(\frac{L}{n}\right)}$$

$$+ \sum_{m=1}^{m=n}\left[\frac{1}{\sum_{l=1}^{l=m} \rho_{e,l}\left(\frac{L}{n}\right) + \rho_{r,m}(\omega)\Big/\left[a_m\left(\frac{L}{n}\right)\right] + \sum_{l=m+1}^{l=n} \rho_{i,l}\left(\frac{L}{n}\right)}\right] \qquad [C\text{-}3]$$

The first term represents the contribution from the MIEC/gas interface at $x = 0$ while the second term corresponds to the contribution from the rest of the MIEC ($0 < x < L$).

As the number of layers, n, approaches infinity (or the thickness of each layer, L/n, approaches infinitesimal), the discretized form of the transmission line model is transformed to a continuous form of the model. In this limit, $R_{e,m}$, $R_{i,m}$, $Z_{r,m}$, $\rho_{e,m}$, $\rho_{i,m}$, $\rho_{r,m}$, a_m, and L/n of an arbitrary element m in the discretized model should be replaced, respectively, with dR_e, dR_i, dZ_r, $\rho_e(x)$, $\rho_i(x)$, $\rho_r(x)$, $a(x)$, and dx for a differential element at a distance x away from the cc/MIEC interface in the continuous model. The differential circuit elements (dR_e, dR_i, and dZ_r) are related to the local properties of the MIEC, $\rho_e(x)$, $\rho_i(x)$, $\rho_r(x)$, and $a(x)$, as follows

$$dR_e = \rho_e(x)\,dx$$

$$dR_i = \rho_i(x)\,dx$$

$$dZ_r(\omega) = \frac{\rho_r(x,\omega)}{a(x)dx} \qquad [C\text{-}4]$$

Accordingly, the summations in Eq. C-1 to C-3 should be replaced with integrals and Eq. C-3 is then transformed to Eq. 3f.

APPENDIX D

Effect of L on G_{rt} for $\rho_e > \rho_i$ and $\rho_i = \rho_e$

MIECs with predominating ionic conduction ($\rho_e > \rho_i$).— Integrating Eq. 9c under the condition that $\rho_e > \rho_i$ (i.e., the rate of ionic transport is faster than that of electronic transport), we arrive at equations similar to Eq. 10 and 12 because of the symmetrical contribution of ionic and electronic transport in the MIEC to G_{rt}. The only modifications needed are to redefine $x = 0$ at the MIEC/el interface and $x = L$ at the cc/MIEC interface and to exchange the position of ρ_i and ρ_e in the Eq. 9c, 10 to 12, and 17. For instance, the $f(L)$ defined by Eq. 11 should be redefined as

$$f(L) = \frac{\rho_r}{a}(\rho_e - \rho_i) - \rho_i\rho_e L^2,\ \rho_e > \rho_i \qquad [D\text{-}1]$$

These changes, however, have no effect on the description of the MIEC electrode or the cell, since Z_{rt} is defined as the total impedance of an MIEC electrode with thickness L. Accordingly, all discussions and conclusions described earlier for the case $\rho_i > \rho_e$ are also applicable to the case $\rho_e > \rho_i$, provided that the position of ionic transport is exchanged with that of electronic transport.

For instance, in the limit of $\rho_i \to 0$ or $\rho_e >> \rho_i$, the characteristic thickness L_c is then determined primarily by the rate of electronic transport and surface reaction. The mathematical description is identical to Eq. 13 to 16, provided that the ρ_is in the equations are replaced with ρ_e.

The only difference between the case of $\rho_i > \rho_e$ and that of $\rho_e > \rho_i$ is the distribution of the reaction at the MIEC/gas interface along the thickness of the electrode. For the case $\rho_i > \rho_e$, the rate of the reaction at MIEC/gas interface (Eq. 1f) increases toward the MIEC/el interface. In contrast, for the case $\rho_e > \rho_i$, the rate of the same reaction increases toward the cc/MIEC interface.

MIECs with equal ionic and electronic conduction ($\rho_i = \rho_e$).—When the rate of ionic transport is identical to the rate of electronic transport, integration of Eq. 9c yields

$$\frac{1}{Z_{rt}(L)} = \left(\frac{1}{2L\rho_i}\right) \ln\left(\frac{\rho_r/a + L^2\rho_i}{\rho_r/a - L^2\rho_i}\right), \quad \rho_i = \rho_e \qquad [D\text{-}2]$$

Differentiating this equation with respect to L, we find that the variation in $G_{rt}(L)$ with L is given by

$$\frac{\partial}{\partial L} G_{rt}(L) = \frac{1}{2L^2\rho_i} \ln\left(\frac{\rho_r/a - L^2\rho_i}{\rho_r/a + L^2\rho_i}\right) + \frac{2\rho_r/a}{(\rho_r/a)^2 - (L^2\rho_i)^2} \qquad [D\text{-}3]$$

Thus, Eq. D-2 and D-3 can be used to determine how the transport (ρ_i or ρ_e) and catalytic (ρ_r/a) properties and the thickness (L) of an MIEC electrode influence the effectiveness of the MIEC/gas interface, $G_{rt}(L)$.

LIST OF SYMBOLS

a	surface area of a porous MIEC electrode per unit volume, cm^{-1}
c_k	molar concentration of species k, mol cm^{-3}
$C_{e,m}$, $C_{i,m}$	capacitance due to polarization of electronic and ionic defects, respectively, in bulk phase of element m ($1 \le m \le n$) in Fig. B-1, F/cm^2
C_{rt}	capacitance of the MIEC/gas interface per superficial area of electrode, F/cm^2
C_{TPB1}	capacitance of TPB1 per superficial area of electrode, F/cm^2
$f(L)$	as defined by Eq. 11, Ω^2 cm^4
F	Faraday's constant, 96,487 C $equiv^{-1}$
G_{rt}	as defined by Eq. 9c, Ω^{-1} cm^{-2}
G_s	as defined by Eq. 9b, Ω^{-1} cm^{-2}
J_k	current density due to motion of defect k, A cm^{-2}
J_{ele}, J_{ion}	electronic and ionic current density, respectively, A cm^{-2}
J_{TPB1}, J_{TPB2}	current density passing through TPB1 and TPB2, respectively, A cm^{-2}
L	thickness of a porous MIEC electrode, cm
L_c	characteristic thickness of a porous MIEC electrode, cm
L_{el}	thickness of electrolyte, cm
N_k	molar flux of species k, mol cm^{-2} s^{-1}
p	porosity of the MIEC electrode, dimensionless
p_{O_2}	partial pressure of oxygen, atm
r	net consumption rate of $V_O^{\bullet\bullet}$ at the MIEC/gas interface, mol cm^{-2} s^{-1}
R	universal gas constant, 8.314 J mol^{-1} K^{-1}
R_b	bulk resistance of a cell ($R_b \approx \lim_{\omega \to \infty} Z_{cell}$), Ω cm^2
R_{ct}, R_{mt}	resistance to charge and mass-transfer, respectively, Ω cm^2
$R_{e,el}$, $R_{i,el}$	resistance to the motion of electronic and ionic defects in the electrolyte, respectively, Ω cm^2
$R_{e,MIEC}$, $R_{t,MIEC}$	resistance to the motion of electronic and ionic defects, respectively, through the entire MIEC as defined by Eq. 3d and 3e, Ω cm^2
$R_{e,m}$, $R_{i,m}$	resistance to the motion of electronic and ionic defects, respectively, in element m ($1 \le m \le n$) in Fig. 4a, Ω cm^2
t_e, t_i	electronic and ionic transference number, dimensionless
t_w	relaxation time constant for mass-transfer, s
T	absolute temperature, K
u_k	absolute mobility of species k, mol cm^2 J^{-1} s^{-1}
v	bulk velocity of gas in the pores of MIEC, cm s^{-1}
x	distance away from the cc/MIEC interface, cm
z_k	number of effective charge carried by defect k, dimensionless
Z_{rt}	impedance to the reaction at the entire MIEC/gas interface and to the transport of the species involved in the surface reaction (as defined by Eq. 3f), Ω cm^2
Z_{cell}	total cell impedance, Ω cm^2
Z_{ee}, Z_{eel}	impedance to electron transfer across cc/MIEC and MIEC/el interface, respectively, Ω cm^2
Z_{ii}	impedance to ion transfer across MIEC/el interface, Ω cm^2
$Z_{r,m}$	impedance to reaction at MIEC/gas interface of element m in Fig. 4a, Ω cm^2
$Z_{r,s}$	impedance to reaction at MIEC/gas interface at $x = 0$ as shown in Fig. 4a, Ω cm^2
Z_{TPB1}, Z_{TPB2}	impedance to the reaction at TPB1 and TPB2 (including the impedance to the mass transfer associated with the reaction), respectively, Ω cm^2
Z_W	Warburg impedance as defined by Eq. 4c, Ω cm^2

Greek

α_a, α_c	anodic and cathodic transfer coefficient, dimensionless
δ	thickness of the electrochemically active layer of a porous MIEC electrode, cm
ϕ	electrostatic potential, V
θ_{cc}	fraction of MIEC surface at $x = 0$ covered by current collector, dimensionless
η	overpotential across an interface due to charge and mass transfer [$\eta_k = \Delta\bar{\mu}_k/(z_kF)$], V
μ_k	chemical potential of species k ($\mu_k = \mu_k^* + RT \ln \gamma_k c_k$), J mol^{-1}
$\bar{\mu}_k$	electrochemical potential of defect k ($\bar{\mu}_k = \mu_k^* + RT \ln \gamma_k c_k + z_kF\phi$), J mol^{-1}
ρ_e, ρ_i	resistivity to motion of electronic and ionic defects in MIEC, respectively, Ω cm
ρ_r	resistivity to the reaction at the MIEC/gas interface (including the resistance to the mass transfer associated with the reaction), Ω cm^2
σ_k	partial conductivity ($\sigma_k = z_k^2 F^2 u_k c_k$) due to the motion of defect k, $\Omega^{-1}cm^{-1}$
τ_s, τ_g	solid-phase and gas-phase tortuosity of the porous MIEC, respectively.

Subscripts

e	electronic
i	ionic
ct	charge transfer
mt	mass transfer

Abbreviations

el	electrolyte
MIEC	mixed ionic-electronic conductor
cc	current collector
TPB	triple-phase boundary
TPB1	TPB between the el, the MIEC, and O_2
TPB2	TPB between the cc, the MIEC, and O_2

REFERENCES

1. *Proceedings of the 1st International Symposium on Mixed and Ionic Conductors,* T. A. Ramanarayanan and H. L. Tuller, Editors, PV 91-12, The Electrochemical Society Proceedings Series, Pennington, NJ (1991).
2. H. J. M. Bouwmeester, H. Kruidhof, and A. J. Burggraaf, *Solid State Ionics,* **72,** 185 (1994).
3. B. C. H. Steele, *ibid.,* **75,** 157 (1995); *ibid.,* **86-88,** 1223 (1996).
4. H. Deng, M. Zhou, and B. Abeles, *ibid.,* **74,** 75 (1994); **80,** 213 (1995).
5. U. Balachandran, J. T. Dusek, S. M. Sweeney, R. B. Poeppel, R. L. Mieville, P. S. Maiya, M. S. Kleefisch, S. Pei, T. P. Kobylinski, C. A. Udovich, and A. C. Bose, *Am. Ceram. Soc. Bull.,* **1,** 71 (1995).
6. M. Liu, (a) *This Journal,* **144,** 1813 (1997); (b) in *Proceedings 1st International Symposium on Mixed and Ionic Conductors,* T. A. Ramanarayanan and H. L. Tuller, Editors PV 91-12, p. 191, The Electrochemical Society Proceedings Series, Pennington, NJ (1991).
7. S. B. Adler, J. A. Lane, and B. C. H. Steele, *This Journal,* **143,** 3554 (1996); *ibid.,* **144,** 1884 (1997).
8. M. Liu and Z. L. Wu, *State Solid Ionics,* Accepted.
9. M. Liu and J. Winnick, *This Journal,* **144,** 1881 (1997).
10. M. Liu and H. Hu., *ibid.,* **143,** L109 (1996).
11. Z. L. Wu and M. Liu, *Solid State Ionics,* **93,** 65 (1997).
12. R. de Levie, *Electrochim. Acta,* **9,** 1231 (1964).
13. R. de Levie, *ibid.,* **10,** 113 (1965).
14. R. de Levie, in *Advances in Electrochemistry and Electrochemical Engineering,* Vol. 6, P. Delahay and C.

W. Tobias, Editors, pp. 329-397, Interscience, New York, (1967).
15. J. R. Park and D. D. Macdonald, *Corros. Sci.*, **23**, 295 (1983).
16. D. D. Macdonald and M. C. H. McKubre, in *Modern Aspects of Electrochemistry*, Vol. 15, J. O'M Bockris, B. E. Conway, and R. E. White, Editors, p. 61, Plenum, New York (1982).
17. M. C. H. McKubre, F. L. Tanzella, and S. I. Smedley, in *Proceedings of the Beta Workshop VIII*, Chester, England (1990).
18. R. H. Bube, *Electrons in Solids*, pp. 217-226, Academic Press, New York (1992).
19. (a) J. R. Macdonald, *J. Chem. Phys.*, **54**, 2026 (1971); (b) *J. Electroanal. Chem.*, **32**, 317 (1971).
20. J. R. Macdonald, *Complex Nonlinear Least Squares Immittance Fitting Program: LOMFP*, University of North Carolina, Chapel Hill, NC (1971).
21. B. Abeles, in *Ceramic Sensors III*, H. U. Anderson, M. Liu, and N. Yamazoe, Editors, PV 96-27, p. 1, The Electrochemical Society Proceedings Series, Pennington, NJ (1997).

Characterizations of Iron-Containing Clay Modified Electrodes and Their Applications for Glucose Sensing

Suh-Ching Shyu and Chong Mou Wang

Department of Chemistry, National Taiwan Normal Univeristy, Taipei 11718, Taiwan

ABSTRACT

An amperometric biosensor was constructed on the basis of ruthenium purple-containing clay and glucose oxidase for the direct assay of glucose. These clay-modified electrodes were characterized by cyclic voltammetry and flow injection analysis techniques. The electrodes were very sensitive to the presence of glucose. Linear calibration curves between 10 μM and 15 mM with an electrode sensitivity of 3.88 μA/M and a detection limit of 10 μM were registered in aerated solutions (pH 5.1). Uric acid, ascorbic acid, and oxygen interfere very little with the detection of glucose. Long-term tests showed these clay electrodes were quite durable, e.g., the electrode sensitivity only decreases by ca. 25% over a period of six weeks.

Introduction

Metal ions are essential to living cells. For example, Na^+, K^+, and Ca^{2+} are important where transport of metabolites and energetic processes are occurring, and transition metals are active catalysts involved in many electron-transport systems.[1,2] Among the transition metals, iron is the principal electron carrier in biological oxidation-reduction reactions.[3,4] Haem groups (Fe^{2+}) and hematin (Fe^{3+}), often associated with protoporphyrin IX, are the coenzymes for a number of redox enzymes. These include catalase, which catalyzes the dismutation of hydrogen peroxide, and peroxidases, which catalyze the reduction of alkyl hydroperoxides. However, the role of iron-containing complexes in the catalysis of biochemical or chemical reactions still needs to be explored.

Recently amperometry-based glucose biosensors have received increases attention due to a clinical demand.[5-8] Research activity has focused on accelerating the slow electron transfer between the reduced glucose oxidase (GOx_{red}) and the probe material and enhancing the sensitivity of the probe to hydrogen peroxide, which is generated by the enzyme-catalyzed reactions.[9-19] To date, excellent catalysts and methods exist for the transduction of hydrogen peroxide,[20] but the reduction of oxygen or oxidation of biologically reducing compounds (ascorbate, uric acid, etc.),[21,22] which might take place at the potentials where hydrogen peroxide is detected must be eliminated or prevented or severe interference may occur.[23-27]

Recently we reported the characterization of iron-containing clays and their application in UV-light recognition[28] and chemical sensing.[29] Many clays contain iron species, and the iron species can be modified with several reagents to influence the surface property of these clay minerals. Although attempts to prepare iron porphyrins on these clays were not successful, ruthenium purple (RP, $Fe_4[Ru(CN)_6]_3$)[30] has been successfully prepared on iron-containing clays, like montmorillonite K10 and montmorillonite KSF, by reacting with $Ru(CN)_6^{4-}$ and shows significant sensitivity to H_2O_2. We report here that a glucose biosensor has been constructed on the basis of the ruthenium purple-containing (clay/RP) particles and glucose oxidase (denoted clay/RP/GOx), which shows high sensitivity to glucose and covers the concentration of glucose from 10 μM to 1 mM in pH 4 to 8. Noticeably, oxygen interferes very little with the detection of glucose. We also investigated the possible interferences caused by other biochemicals (uric acid and ascorbic acid) on glucose detection.

Experimental

Chemicals and reagents.—H_2SO_4 and K_2SO_4 (99%) were supplied by Merck. Glucose oxidase (GOx, type VII from Aspergillus Niger; 137,000 units/g), bovine serum albumin (BSA), *L*-ascorbic acid, uric acid, β-*D*-glucose, and glutaraldehyde were purchased from Sigma. Montmorillonite K10, potassium hexacyanoruthenate(II), *o*-phenylenediamine, and hydrogen peroxide were obtained from Aldrich. The preparation of clay followed procedures described elsewhere.[28] The clay/RP particles were prepared by reacting 9 mg of ruthenium hexacyanide with 100 mg of the clay in 20 ml sulfuric acid (0.2 mM) with constant stirring for 4 h.[29]

Electrode preparations.—Clay-modified electrodes were fabricated on conductive SnO_2 glass (indium-doped 0.7 mm thick, 20 Ω/cm²; Delta Technologies). Typically, 20 μl/cm² of a clay slurry (1 g/liter water, denoted solution A) was first cast on the glass squares and dried at an ambient temperature (ca. 25°C). After this, 20 μl/cm² of a GOx solution (denoted solution B) was cast onto the resulting glass squares (denoted sandwich-type clay electrodes). Solution B contained 5 ml GOx (25 g/liter water), 3 ml of the aqueous glutaraldehyde (GA, 4%), and 5 ml BSA (20 g/liter water). Polymethyl methacrylate (PMMA) or poly(*o*-phenylenediamine) (PPD) were also used instead of glutaraldehyde as the enzyme immobilizer to fabricate the clay electrodes. In the case of PMMA, a thin film of PMMA (30 μl/cm², 10 g/liter in ethyl acetate) was applied onto the glass squares after the incorporation of GOx. With PPD, a procedure similar to that described by Malitesta et al. was followed.[31] Typically, 100 mg of GOx was mixed with 10 ml *o*-phenylenediamine (5 mM) prior to immobilization. Films were grown for 10 min at a constant applied poten-